J. COMBIN. MATH. COMBIN. COMPUT. 127b (2025) 8833--8851

Journal of Combinatorial Mathematics and Combinatorial Computing
www.combinatorialpress.com/jcmcc

Combinatorial Press

Construction of Intelligent Power Preservation System under the Integration of Internet of Things and Artificial Intelligence

Yu Jiang[1], Yu Wang[2,✉], Shucui Tan[2], Xiongyong Jiang[2], Liangyuan Mo[2]

[1] *Nanning Power Supply Bureau of Guangxi Power Grid Co., Ltd., Nanning, Guangxi, 535000, China*
[2] *Yulin Power Supply Bureau of Guangxi Power Grid Co., Ltd., Yulin, Guangxi, 537000, China*
[3] *Qingxiu Power Supply Branch of Nanning Power Supply Bureau, Nanning, Guangxi, 535000, China*

ABSTRACT

Distribution network line project acceptance is a key link in the quality control of distribution network line project, an important factor affecting the safe and stable operation of the distribution network, which directly determines the level of safe operation of the distribution network. In this paper, for the distribution network line manual acceptance time-consuming and laborious, rare quality defects found rate identification rate is low and other issues, to carry out visual positioning and image recognition based on the distribution network drone automated acceptance technology research. In order to optimize the spatial positioning, attitude sensing and target tracking of the UAV, five coordinate systems, including the world coordinate system, body coordinate system, and photocentric coordinate system, are selected for spatial transformation. Based on the visual localization of the UAV, the path planning algorithm for UAV distribution line inspection combined with the path acquisition scheme is proposed. Gaussian denoising and histogram equalization are performed on the UAV inspection collected images, and Sarsa reinforcement learning algorithm is applied to train the samples to improve the automatic identification capability of safety hazards and other security hazards in the distribution network inspection. Visualization and analysis of UAV distribution line inspection path. Combine the distribution network defects dataset for optimal training strategy selection for distribution networks. The automatic identification algorithm for distribution network defects proposed in this paper achieves a mAP value of 79.60% in the target detection experiment. And in multiple dynamic path planning, the UAV nodes are able to accomplish the path planning tasks in different environments.

Keywords: sarsa algorithm, gaussian denoising, histogram equalization, UAV inspection, automatic defect identification, distribution network line

✉ Corresponding author.
E-mail address: Wangyu_1975@outlook.com (Y. Wang).
Received 05 February 2024; Revised 12 April 2024; Accepted 05 December 2024; Published Online 16 April 2025.
DOI: 10.61091/jcmcc127b-485

1. Introduction

Along with the deepening of economic and social development, China's comprehensive national strength has increased significantly, and more and more economic, political and cultural events are chosen to be held in China. As a "great power", the State Grid Corporation of China (SGCC) has incorporated the construction of corporate social responsibility into the major deployment of the "two first-class" strategy, and it is not only the most important business responsibility of power supply enterprises to ensure power supply for various major activities, but also the needs of power supply enterprises to adapt to the new economic era and the new normal of power protection [1-4]. After years of informationization construction, State Grid Corporation has formed a complete informationization construction system by relying on information systems within the profession, but the ability of cross-professional integration and sharing is insufficient, the process of cross-professional collaboration is imperfect, the granularity of enterprise management is not fine, the boundaries of management are unclear, the rules of apportionment are not standardized, and the level of information resource utilization is low. Along with the construction work of electric power Internet of Things, each specialty will break the information barriers and realize the data interaction and information sharing between systems, so as to promote the unified deployment and horizontal synergy of professional departments [5-8].

The core value of the data center lies in the precipitation of common and reusable data assets, and the power supply system based on the data center breaks the information barriers between business systems, realizes professional information interconnection, and further improves the platform's panoramic perception ability, data fusion ability, information interaction ability, key monitoring ability and auxiliary decision-making ability, effectively improves the power supply monitoring ability and emergency response speed of the power grid, and ensures the safe and stable operation of the power system during the special guarantee period of power supply. It provides strong information support for promoting the reform of power grid production mode and the innovation of management mode [9-12].

With the development of intelligent power preservation technology, the tasks of primary and secondary power preservation are increasing. In order to improve the level of power preservation, the intelligent and scientific power preservation system and decision-making model is established by using intelligent and scientific methods in conjunction with the current construction project construction dynamic model, and the methods of on-site monitoring and power safety detection are used to achieve intelligent power preservation decision-making and optimal scheduling [13-15]. Fiber-to-the-building (FTTB) is an access scenario that uses digital broadband technology to realize optical broadband to each user through twisted pair cables, which can better provide multimedia interactive power services. Through the design of intelligent power preservation decision-making based on reinforcement learning in FTTB scenarios, the intelligent power preservation decision-making ability can be improved and the efficiency of power preservation work can be enhanced [16-18]. In the design of intelligent power preservation decision-making system, the algorithm control module and hardware composition module of intelligent power preservation decision-making are established by combining the application system and IoT platform, and the embedded design method is adopted for intelligent power preservation decision-making control [19-20]. In traditional methods, artificial game control methods or evolutionary game control methods are mainly used for intelligent power preservation decision-making, and the intelligence level of power preservation decision-making by these methods is not high, in this regard, it is necessary to explore the intelligent power preservation decision-making methods based on reinforcement learning in FTTB scenarios [21-22].

This paper analyzes the problems encountered in the quality acceptance of distribution network lines, and points out the importance of the acceptance of distribution network line engineering for the quality control of distribution network line grid engineering. The distribution network line inspection goal is formulated, and five coordinate systems are selected for spatial transformation in order to optimize the precise perception of spatial position and spatial attitude by UAV equipment. Combined with the path collection data, the path planning algorithm in the UAV distribution line inspection path planning and autonomous inspection method based on key coordinate points is proposed. In order to reduce the impact of illumination on inspection images, Gauss filter and histogram equalization algorithm are used to process the images in the preliminary work. Sarsa reinforcement learning algorithm is used to strengthen the performance of feature extraction and optimize the automatic identification technology of distribution network inspection defects. Establish the distribution network intelligent inspection control role control platform. Separate performance tests are performed to verify the hands-on performance of the algorithms proposed in this paper.

2. Key technologies for intelligent inspection operations in distribution networks

2.1. Description of the problem

Distribution network line quality acceptance is an important factor to ensure the safe and stable operation of the power grid. For a long time relying on sampling and manual way to carry out distribution network line project acceptance work, there are the following problems:

1) Manual acceptance is time-consuming and laborious. For the distribution network line is long, equipment, artificial acceptance, manual acceptance needs to spend a lot of manpower and material resources.

2) The efficiency of manual acceptance is low and poor. Distribution network infrastructure line acceptance, manual workload, and equipment information matching is easy to error, incomplete project statistics, the effect is often not up to expectations.

3) Narrow coverage. Manual acceptance is difficult to reach the fish ponds, lakes and other multi-scenario geographic areas of the distribution network line acceptance work, resulting in the quality of the distribution network line can not be guaranteed.

4) Poor quality of archived data. Due to the initial and completion engineering changes, the as-built drawings and project volume changes, tower type, equipment inventory, manufacturer categorization and other data can not be effectively archived.

Drone distribution network engineering acceptance application, research and application of the unit or company is still relatively small. Such as line project acceptance, the use of “machine patrol alternative” to improve professional productivity, can effectively make up for the short board of the traditional operation and maintenance mode of distribution lines, distribution network project construction cycle is short. Can make full use of the drone hovering in the air to take pictures and real-time transmission back to the characteristics of the breakthrough of the traditional manual acceptance of low efficiency, acceptance of the existence of blind areas of the bottleneck. Compared with transmission lines, the length of distribution overhead lines is shorter, the tower is lower, the electromagnetic radiation of the line is smaller, the requirements for the anti-interference ability and deviation correction ability of the drone are lower, and the distance of the electrical equipment on the distribution tower is closer. UAV shooting a photo can directly cover three phases, and the shooting accuracy and the number of shooting requirements are much lower than that of transmission lines. However, the distribution line corridor situation is complex, there are cross-crossing, high-altitude obstacles, etc., and some of the lines are in densely populated areas with poor take-off conditions, which are all difficult problems that need to be researched.

2.2. Necessity analysis

Distribution network line project acceptance is a key link in the quality control of distribution network line grid project, is an important factor affecting the safe and stable operation of the distribution network, which directly determines the level of safe operation of the distribution network. Distribution network completion project and the initial set in the path, the amount of work compared to the verification is more time-consuming, manpower and material resources consumption. Construction technology defects, equipment type mismatch and other engineering quality problems will be for the distribution network safety and stable operation of buried hidden trouble.

At present, the South Network UAV has been applied to a large number of transmission, substation and distribution professional daily equipment inspection work, forming a more mature application. In the field of infrastructure engineering, relevant research is also being gradually carried out. However, the data collection method of UAV is still mainly based on manual control by the pilot. The collected data are confirmed sheet by sheet by means of manual review. Subsequently, with the significant development of artificial intelligence technology, the shift from manual control to automatic flight of UAVs and from manual analysis to intelligent analysis of data will be the mainstream trend. Therefore, a safe, advanced, scientific and efficient way of line project quality acceptance is needed.

Distribution network drone automation acceptance is an efficient, intelligent, new acceptance mode, highly concentrated drone, visual recognition, OCR recognition, positioning navigation, geographic information and many other cutting-edge results, representing the development direction of intelligent, integrated, automated acceptance.

2.3. Intelligent inspection technology for distribution network line drones

2.3.1. Distribution network line inspection objectives:

1) Ensure the quality of power supply. The primary goal of distribution network line inspection is to guarantee the quality of power supply and ensure the stability and reliability of power supply. Through inspection, line faults, loose joints, insulation aging and other problems can be found and solved in a timely manner to avoid power supply interruptions, voltage fluctuations and power loss, and to improve the quality and reliability of electricity for users.

2) Prevent accidents. Regular inspection of distribution network lines can identify potential safety hazards and failure risks. Timely treatment of line problems reduces the occurrence of accidents such as electrical fires, short circuits, leakage and electrocution, and protects personal safety and property safety.

3) Improve equipment reliability. Distribution network line inspection can timely detect problems such as equipment damage, aging and wear, and take timely measures to repair, replace or reinforce the equipment to improve its reliability and life. Through inspection, the grounding, insulation and connectors of the line can be inspected, and problems can be dealt with in time to avoid the spread and deterioration of faults.

2.3.2. Drone inspection technology. The principle of UAV inspection technology refers to the use of UAV flight platforms and related equipment, combined with route planning, sensor technology and data processing and other technical means to implement efficient and comprehensive line inspection [23-24]. Its main principles include UAV flight platform, sensor use and data processing and other aspects of technology.

1) Visual localization of UAV. For the quadcopter UAV, its power equipment inspection process requires precise perception of its spatial location and air attitude. The UAV with video recognition function contains multiple coordinate systems, and it is necessary to carry out coordinate system space transformations under the coordinate system space for the world coordinate system, body coordinate system, optical center coordinate system, image plane coordinate system, and image pixel coordinate system.

In order to facilitate the analysis and calculation, five coordinate systems are selected and transformed to simplify the principles of spatial localization, attitude sensing, and target tracking of rotary-wing UAVs.

The external image is converted into a digital signal by the camera mounted on the body through photoelectric conversion and stored in the computer and processed in the form of a matrix for subsequent operations. Assuming that the acquired image digital signal matrix scale is $M \times N$, M and N represent the number of pixel rows and columns of the image, respectively, and the value of each element in the matrix represents the exposure information of the corresponding pixel point. The coordinate values of each point of the object in the image pixel coordinate system $O_i - uv$ can be transformed by the image plane coordinate system $O - XY$, which is calculated as follows:

$$\begin{cases} u = \dfrac{x}{d_x} + u_0 \\ v = \dfrac{y}{d_y} + v_0 \end{cases} \tag{1}$$

where x and y are the position of a point of the object in the image plane coordinate system. d_x and d_y are the reciprocal of the camera's pixel density and are the physical dimensions of each pixel point on the x- and y-axis, respectively. u and v denote the coordinates of the position of the pixel in the array. u_o and v_o are camera intrinsic parameters and are the coordinate values of O points in the image pixel coordinate system.

Cameras are used as a tool for acquiring image information, and the quality of their imaging affects subsequent image processing. Through the camera's imaging method and its mathematical expression, a mapping relationship between the three-dimensional scene and the pixels can be derived. Through this mapping relationship, it is possible to reduce the pixels in an image to three-dimensional space. If all the pixels of a series of images are all reduced to the entire 3D space, the surface of the entire scene can be reduced.

The camera imaging model can be divided into two parts according to the physical principles, which are the pinhole model and the charge-coupled device (CCD) camera imaging model. Among them, the pinhole camera imaging model and the CCD camera imaging model are used to characterize the transformation relationship from the spatial point coordinates under the photocentric coordinate system of the UAV to the image plane coordinate system and the image pixel coordinate system, respectively.

The accurate estimation of the position and attitude of the inspection UAV by the distribution network equipment is the prerequisite and foundation for realizing the autonomous flight and visual inspection of the distribution network equipment inspection UAV. In the article, a computer vision-based method is used to estimate the position and aerial attitude of the UAV. The workflow of the method consists of three steps including feature extraction, 3D pose reconstruction and angle calculation. The input to the system is a video image (essentially an image sequence) captured by a camera. Based on the five coordinate system mathematical models established in the previous section, the aerial pose of the rotary UAV can be obtained by processing the video images.

The coordinate value of any point in the external view in the world coordinate system can be transformed to its coordinate value in the photocentric coordinate system inside the camera by rigid body coordinate transformation, which is calculated as follows:

Assume that a point in the external environment has a coordinate value of $\left(X_w, Y_w, Z_w\right)$ in the world coordinate system:

$$\begin{bmatrix} X_c \\ Y_c \\ Z_c \end{bmatrix} = R \begin{bmatrix} X_w \\ Y_w \\ Z_w \end{bmatrix} + T \tag{2}$$

where (X_w, Y_w, Z_w) and (X_c, Y_c, Z_c) are the coordinate values of a point in space in the world coordinate system and photocentric coordinate system, respectively.

Equation (3) is expressed in chi-square coordinates as:

$$\begin{bmatrix} X_c \\ Y_c \\ Z_c \\ 1 \end{bmatrix} = \begin{bmatrix} R & T \\ 0 & 1 \end{bmatrix} \begin{bmatrix} X_w \\ Y_w \\ Z_w \\ 1 \end{bmatrix} \tag{3}$$

where submatrices R and T are 3×3 -matrix and 3-dimensional column vectors, respectively, representing the rotation and translation matrices of the point transformed from the world coordinate system to the photocentric coordinate system.

Substituting into Eq. (3), the coordinate value of a point in the external scene in the world coordinate system can be obtained by the coordinate value in the image pixel coordinate system obtained by the transformation of the photocentric coordinate system and the image plane coordinate system, which is calculated as follows:

$$Z_c \begin{bmatrix} u \\ v \\ 1 \end{bmatrix} = K \begin{bmatrix} R & T \end{bmatrix} \begin{bmatrix} X_w \\ Y_w \\ Z_w \\ 1 \end{bmatrix} \tag{4}$$

The position estimation of a rotary UAV is determined based on a computational model of the transformation relationship between the world coordinate system and the airframe coordinate system, so it is necessary to establish the equations of the transformation relationship between the two coordinate systems mentioned above that contain the airframe position information:

$$\begin{bmatrix} x_\alpha \\ y_\alpha \\ z_\alpha \end{bmatrix} = \begin{bmatrix} \cos\theta\cos\psi & \cos\theta\sin\psi & -\sin\theta \\ \sin\theta\cos\psi\sin\phi - \sin\psi\cos\phi & \sin\theta\sin\psi\sin\phi + \cos\psi\cos\phi & \cos\theta\sin\phi \\ \sin\theta\cos\psi\cos\phi + \sin\psi\sin\phi & -\sin\theta\sin\psi\cos\phi - \cos\psi\sin\phi & \cos\theta\cos\phi \end{bmatrix} \begin{bmatrix} x_x \\ y_y \\ z_z \end{bmatrix} \tag{5}$$

After the rotation transformation from the world coordinate system to the airframe coordinate system, the transformation matrix of three parameters containing the airframe position information can be obtained. Then the matrix equation can be solved to complete the position estimation of the rotary UAV.

2) UAV autonomous inspection path planning. In the path planning stage, in order to improve the flexibility of autonomous inspection path planning, this program combines the path acquisition

program with the key coordinate point-based UAV distribution line inspection path planning and path planning algorithm in the autonomous inspection method.

Determine the base towers for which path planning is required, and determine the type of set of towers selected by the user. Set A as the consecutive selection of towers, B as the span between towers is within two base towers, and C as the span between towers is more than two base towers. Select the UAV path planning flight mode in the corresponding mode according to the span between the towers. If the tower set type is A, then omit the landing point of $1,2,3,4,\ldots,n-1$ base tower (n is the number of inspection towers), connect the back-sequence connection point of No. 1 tower with the front-sequence connection point of No. 2 tower, and so on until the back-sequence connection point of No. n tower. Finally, it will land on the landing point of tower No. n.

If the tower set type is B, after completing the missing tower in the middle, after path planning according to the path planning algorithm of continuous tower, all the actions on the path points of the missing tower are deleted, and fly through directly, so as to ensure that the path of the UAV autonomous inspection is safe and controllable.

If the type of the pole tower collection is C, in order to save fuel, select two pole towers 15m above the highest point from the ground as the front and rear sequence connection points, and then connect the front and rear sequence number connection points of the front and rear pole towers in turn.

a. Recalculate the path point elevation. Since the height of the path point during autonomous flight is relative to the height of the takeoff point, the elevation of the path point needs to be recalculated as in Equation (6):

$$h_{\text{Pathpoints}} = H_{\text{Pathpoints}} - H_{\text{Takeoff point}} \tag{6}$$

where h is the relative altitude and H is the ground altitude.

1) Calculate the total flight distance.

Project the planned sequence of path points (B,L,H) onto the Gaussian plane of (x,y,h).

Calculate the total horizontal flight path as in equation (7):

$$S_h \sqrt{\sum \left(x_i - x_{i-1}\right)^2 + \left(y_i - y_{i-1}\right)^2} \tag{7}$$

2) Calculate the total climb and landing distance as in equation (8):

$$S_v = \sum \left|h_{i+1} - h_i\right| \tag{8}$$

3) Calculate the total flight time. The total horizontal flight time is estimated at a speed of $8m/s$. The horizontal flight time is given in equation (9):

$$t_h = s_h / 8 \tag{9}$$

4) Climbing and landing speeds are estimated at the rate of $2m/s$, then the climbing flight time is as in equation (10):

$$t_v = s_v / 2 \tag{10}$$

5) Calculate the total flight time as in equation (11):

$$t = t_h + t_v \tag{11}$$

6) Judgment of path reasonableness based on total flight time, total distance traveled, and UAV flight capability.

2.4. Automatic identification of defects in distribution network inspection

2.4.1. Image processing. Usually, illumination is easy to have a large impact on the images collected by inspection. In order to reduce the image in the process of generating and transmitting due to noise and interference and other unfavorable factors, the noise in the inspection acquisition image through Gauss filter implementation of denoising. The image is enhanced using histogram equalization enhancement algorithm to improve its contrast and solve its overexposure to complete the preliminary work of image preprocessing [25]. Enhanced samples enhance the training dataset, increase the amount of data in the collection and the generalization ability of the model, and reduce the risk of fitting.

2.4.2. Sarsa reinforcement learning algorithm training. The convolutional neural network model utilizes the TF platform to annotate 10,000 of the patrol acquisition images, of which 8,000 are used for training and 2,000 for validation, to generate a model for extraction against the target monitoring region.

1) Image segmentation:

(1) Background model. Parameter pairs H, I and S are used to describe the color characteristics of the color model, respectively, where H denotes the hue to describe the wavelength of the color. I denotes the color brightness. S represents saturation, which is used to describe the degree of color. The model transformation $(RGB \to HSI)$ is performed for the processed image to obtain the pixel values according to the formula, i.e:

$$I(i,j) = \frac{1}{3}[R(i,j) + G(i,j) + B(i,j)] \tag{12}$$

The mean value of the background image brightness is:

$$I_m = \frac{1}{k} \sum_{J(i,j) \neq 0} I(i,j) \tag{13}$$

where k is used to describe the number of pixel points whose brightness is not equal to zero.

(2) Normalization process foreground conversion. Gamma conversion of the gray value of the input image using nonlinear operations, prompting the relationship of the image gray value between the output and the input two is:

$$y = x^{\gamma} \tag{14}$$

where γ represents the standard value of gray scale.

When γ>1, the region where the gray scale is stretched is the region with higher brightness, and the compressed region is the region with lower brightness, and the overall image brightness shows a trend of more dimness.

When γ<1, the gray scale is stretched in areas with lower brightness and compressed in areas with higher brightness, and the overall image brightness tends to be brighter.

Image brightness is too high and too low is not desirable, so when the image brightness is more than 128, the image brightness needs to be reduced using Gamma conversion, on the contrary, the brightness needs to be increased, the conversion parameter formula is:

$$\gamma = \frac{I_m}{128} \tag{15}$$

2) feature extraction based on the super red algorithm. For the detection of defects shown in the foreground target, the target features in the defective region should be highlighted to show in red is called the ultra-red method, the algorithm can effectively distinguish the defective region red features are realized by the weighted combination method $2R - G - B$. Its red region gray value calculation formula is:

$$E_x R(i,j) = 2R(i,j) - G(i,j) - B(i,j) \tag{16}$$

3) Sarsa reinforcement learning algorithm. Sarsa reinforcement learning algorithm is used to train the samples so that they have the ability to automatically identify defects such as tree barriers, equipment and safety hazards during distribution network inspection [26-27].

Under the current policy conditions, the value function of the a action in the s state is estimated using $Q(s,a)$ the process of Sarsa's algorithm, Eq:

$$Q(s_t,a_t) \leftarrow Q(s_t,a_t) + a_1\left[\lambda_{t+1} + \lambda Q(s_{t+1},a_{t+1}) - Q(s_t,a_t)\right] \tag{17}$$

In the formula, $a(0 \le a \le 1)$ represents the learning rate of reinforcement learning speed control, the learning rate is proportional to the convergence speed, when the learning rate is larger, although the convergence speed is also relatively faster, but at the same time there are easy to oscillate the problem. $\lambda(0 \le \lambda \le 1)$ represents the discount factor of reinforcement learning on the degree of attention to recent work, the discount factor is proportional to the degree of attention. All the variables contained in Eq. (17) are constructed as $s_t, a_t, \lambda_{t+1}, s_{t+1}, a_{t+1}$ quintuples.

The modulo system based on the composition of rules (R), inputs (n) and outputs (1) is described as:

$$\begin{aligned} &R_1 : if\ x_1\ is\ L_1 \\ &and\ x_n\ is\ L_{in} \\ &Then : \left(a_i with\ \omega^{in}\right) \\ &or\left(a_{im}\ with\ \omega^{im}\right) \end{aligned} \tag{18}$$

where the input vector $S = X_1 \times X_2 \times \cdots \times X_n$ belongs to n dimensions. The convex set corresponding to rule i is $L_i = L_{i1} \times L_{i2} \times \cdots \times L_{im}$, m denotes the number of discrete actions of the rule, rule i is denoted by a_{ij} in the j th action, and the approximation function value is denoted by ω^{ij}. The candidate actions in the rule are in discrete form, and the final input action is continuous, and the continuous action $a \in \left[\min_{ij}(a_i), \max_{ij}(a_{ij})\right]$, and the odds of candidate action being adopted by rule i in the S_i state condition is calculated by the formula:

$$P(a_{ij}) = \frac{\exp\left[\mu_i(s_t)\omega^{ij}/T\right]}{\sum_{i=1}\exp\left[\mu_i(s_t)\omega^{ij}/T\right]} \tag{19}$$

where the value of the affiliation function for rule i is denoted by $\mu_i(S_i)$, and the temperature parameter T is greater than zero, which is the degree of stochastic control of the selection made for the action, assuming that the selected action is a_{ii+} and the approximation value is ω^{ii+}, the output is calculated as follows:

$$a_t(s_t) = \sum_{t=1}\mu_i(s_t)a_{ii+} \tag{20}$$

The approximation function value is calculated as:

$$\hat{Q}_t(s_t,a_t) = \sum_{t=1}\mu_i(s_t)\omega^{ii+} \tag{21}$$

Obtain the action selection probability according to Eq. (19), Eq. (20) and Eq. (21), i.e:

$$P(a) = \frac{\exp \hat{Q}(s,a)/T}{\sum_{s=1} \exp \bar{Q}(s,a)/T} \tag{22}$$

The formula for updating the weights is:

$$\Delta\omega_{t+1}^{ij} = \begin{cases} a_{t+1} \times \Delta\hat{Q}_t\left(s_t, a_t\right) \times \mu_i\left(s_t\right) & \mathit{ifj} = i^+ \\ 0 & \mathit{otherwise} \end{cases} \tag{23}$$

where the error generated by the approximation is denoted by $\Delta\hat{Q}$ and the error is calculated by Eq:

$$\Delta\hat{Q}t\left(s_t, a_t\right) = \lambda_{t+1} + \gamma\hat{Q}t\left(s_{t+1}, a_{t+1}\right) - \hat{Q}t\left(s_t, a_t\right) \tag{24}$$

2.5. Intelligent inspection control operation management platform

2.5.1. Functional Requirements of Intelligent Inspection Integration Platform. The substation intelligent inspection integration platform designed in this paper will meet the following requirements:

1) Adopt standardized test data acquisition communication protocols in accordance with regulations. The transmission of on-site inspection data is subject to standardized data format constraints. The communication protocol supports the mainstream inspection instruments on the market and ensures the uniformity and standardization of the output data of the same test project, thus providing a strong support for the efficient use of data.

2) Intelligent inspection platform can produce “wireless self-organizing network”, the field inspection instruments can be connected to the network or Bluetooth and other ways to transmit data. This paper focuses on the transformation of the inspection instrument with wireless transmission capability, does not meet the function of the instrument will be in the follow-up work of communication transformation.

3) Mobile console (PAD and cell phone) can be connected to the wireless network generated by the intelligent inspection platform, inspection personnel through the mobile device to control the inspection platform, on-site inspection work process guidance, mobile devices are only positioned as a display of the inspection platform, does not have the function of data analysis.

4) Intelligent inspection platform internal storage of rich equipment historical data and algorithmic models, on-site power patrol, you can use the platform to store resources for data analysis, inspection data for horizontal and vertical comparison and analysis, abnormal data can be further advanced algorithmic analysis, in advance of the discovery of latent defects and the state of the deterioration of the trend of diagnosis of equipment failures in order to help timely on-site equipment operation and maintenance work.

5) Intelligent inspection integration platform can be connected to the management side through the power private network or GPRS (operator's professional network), and the platform uploads inspection data and inspection results with one click, while the platform can obtain richer data resources from the back-end management side and download updated advanced diagnostic algorithms, thus realizing two-way resource sharing.

2.5.2. Intelligent inspection integrated platform overall program. The intelligent inspection integration platform studied in this paper serves as an “intelligent transit body”, which can provide support and guidance for on-site work specification by calling the calculations and data on the management side. At the same time, it can obtain the inspection data obtained by the inspection instrument and has certain data analysis capability. A complete workflow from data collection to result generation is formed between field data collection device, intelligent inspection integration platform and management terminal, and the inspection work at substation site becomes more intelligent and integrated.

Substation inspection work is generally only in the field in accordance with the test steps for testing, recording test data in the background after the data processing and analysis. The intelligent inspection integration platform inspection tasks from the test operation, data acquisition to data analysis and other aspects can use the platform completely in the field to achieve, enhance the standardization of inspection work and inspection mode of intelligence. By analyzing the functional requirements of the intelligent inspection integration platform and the interface relationship. The overall architecture of the platform is designed, and the architecture of the intelligent inspection integration platform is divided into the application layer and the kernel layer. The architecture design of the intelligent inspection integration platform is shown in Figure 1.

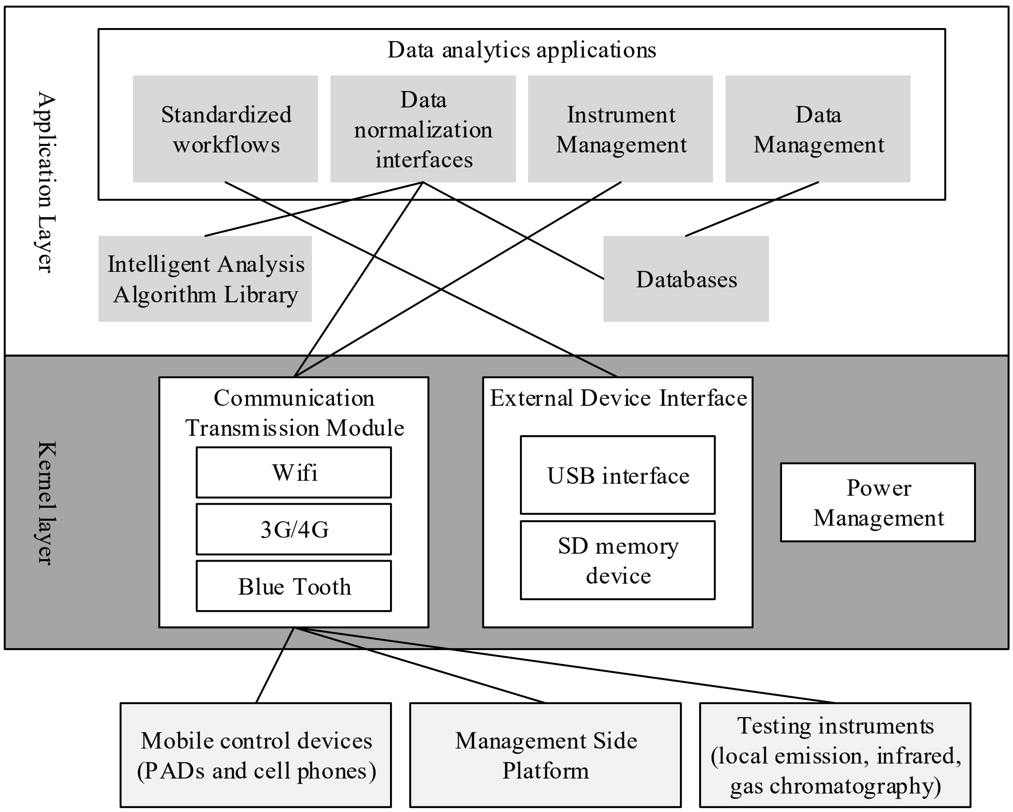

Fig. 1. Architectural design of the integrated platform of intelligent inspection

3. Distribution network intelligent inspection technology performance testing

3.1. Drone Distribution Line Inspection Path Planning

3.1.1. Experimental environment and design. The simulation experiments are based on Python platform, and the experiments mainly present the proposed real-time planning algorithm with visualization results. Several different sets of start point and target point coordinates are selected for the experiment. In addition, different experimental environments are set up, which are realized by controlling the shapes of obstacles, such as circles and rectangles. The motion states of the obstacles, such as irregular movement and stationary state.

Experimental environment: Windows 10, Intel(R) Core(TM) i7-7400 CPU @3.00GHZ (4 CPUs), ~3.0GHZ, 8G RAM.

Compilation tool: PyCharm2023.

Parameter settings: the environment size is 60×60, and the range of both X and Y axes is [-15,15]. The values of α and β are set to 0.1 and 2. The weighting factors ω_1 and ω_2 are set to 0.3 and 0.7. The maximum steering angle of the UAV is 60°. The maximum number of iterations was set to

6000.

The maximum number of reconnections is the start point is set to green, the target point is set to red, and the moving multiple obstacles are shown in gray, where the radius size of the circular obstacles is 2, and the rectangular obstacles have dimensions of 3 × 3, 1 × 6, 4 × 1, and 2 × 2. The black color represents the position of the UAV, where the search tree is shown in gray, and the optimal path for planning is shown in blue.

3.1.2. Visualization results. The visualization experiments select different start and target nodes and different dynamic environments to test the stability of the algorithm operation. The experimental results show that the UAV nodes are capable of accomplishing the path planning task in different environments in all the 30 experiments conducted. Finally, from the multiple sets of experiments, the coordinates of the start point are selected as (-11, -11) and the coordinates of the target point are selected as (11, 11).

It is guaranteed that the UAV node carries out the maximum movement in the environment, and the whole planning process is shown in Fig. 2. Figure (a) shows the initial path obtained by the algorithm at the beginning of the algorithm. The original path is blocked due to the movement of obstacles, which initiates the path replanning process. Figures (b)~(d) show the 2nd, 4th, and 30th obstacle update paths, respectively.

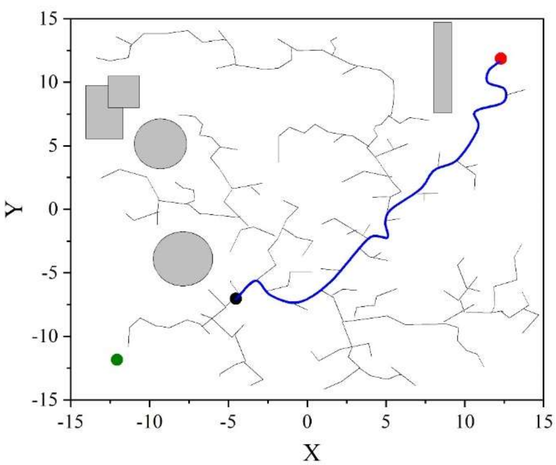

(a) Initial obstacle update

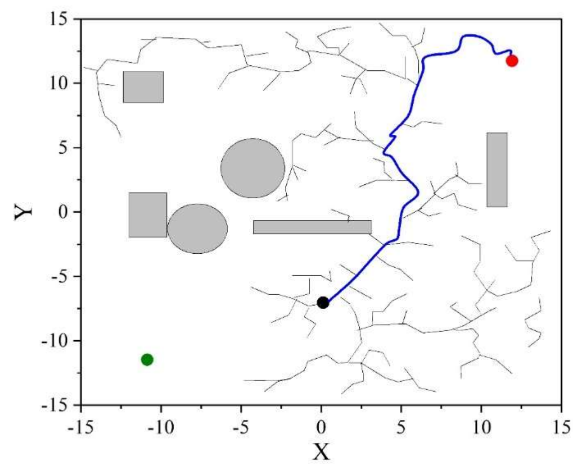

(b) The second obstacle is updated

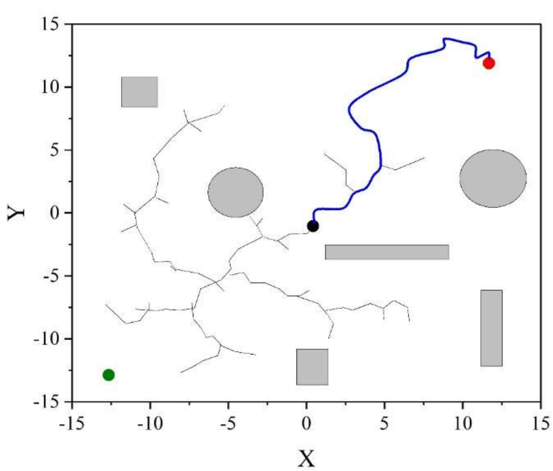

(c) The fourth obstacle is updated

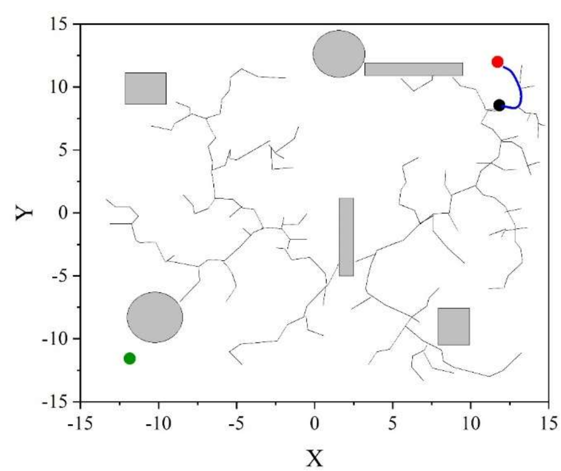

(d) The 30th obstacle is updated

Fig. 2. Real-time path planning in dynamic environment

3.2. *Reinforcement learning based automatic identification of defects in distribution network inspection*

3.2.1. Image processing. In order to validate the algorithm, the following lena image of size 512*512 pixels and gray level 256 is selected as a test sample. The related peak signal-to-noise ratio and the processing time of this algorithm are shown in Table 1. = At 10, 20, 30, 40, 80, 100, the PNSR of the denoised image according to the method of this paper is 3.462dB, 4.583dB, 7.889dB, 8.201dB, 8.794dB, and 12.119dB higher than that of the PSNR of the image containing the noise, respectively.

In order to validate the algorithm, the following lena image of size 512*512 pixels and gray level 256 is selected as a test sample. The associated peak signal-to-noise ratio and the processing time of this algorithm are shown in Table 1. σ=10, 20, 30, 40, 80, 100, the PNSR of the denoised image according to the method of this paper is 3.462dB, 4.583dB, 7.889dB, 8.201dB, 8.794dB, 12.119dB higher than that of the PSNR of the noisy image, respectively. In addition, it can be seen that the Gaussian denoising algorithm utilized in this paper spends less time on the entire denoising process, which has a high efficiency ratio.

Table 1. The correlation of peak signal-to-noise ratio and the time of this algorithm

σ	PSNR/dB				This algorithm CPU time (s)
	Primordial	Mean filtering	Wiener filtering	This algorithm	
10	32.415	33.754	35.629	35.877	1.8553
20	29.076	31.661	33.213	33.659	1.6417
30	23.332	30.214	30.857	31.221	1.4261
40	19.804	28.657	27.117	28.005	1.0399
80	17.553	25.829	25.364	26.347	0.9813
100	12.087	21.203	23.159	24.206	0.8596

Two metrics, Peak Signal to Noise Ratio (PSNR) and Structural Similarity (SSIM), are used to evaluate the effectiveness of the histogram equalization algorithm. The larger the value of peak signal-to-noise ratio, the better the noise immunity of the image. Structural similarity measures the similarity of two images in three dimensions: brightness, contrast and image structure. The closer the value is to 1, the better the similarity of the two images.

The experimental results are shown in Table 2, where 4 data are randomized 4 scenes. After the experiments, it is proved that the algorithm in this paper improves both PSNR and SSIM relative to the original images, and the PSNR of the four scenes is improved by 11.297%, 4.851%, 3.984%, 3.351%, respectively.The SSIM of the four scenes is improved by 0.0291, 0.3049, 0.0832, 0.0555, respectively.The average improvement of PSNR is 5.871% and SSIM is improved by 11.82% on average.

Table 2. Experimental results

	Scene number	Primordial	Algorithm in this paper
PSNR/dB	Scene1	47.366	58.663
	Scene2	33.254	38.105
	Scene3	29.637	33.621
	Scene4	35.935	39.286
PSNR	Scene1	0.9212	0.9503
	Scene2	0.6736	0.9785
	Scene3	0.3325	0.4157
	Scene4	0.6208	0.6763

3.2.2. Results of inspection defect identification. The defective target detection dataset is obtained from Southern Power Grid with the number of 352 images. The images of this dataset are preprocessed separately. 80% is randomly selected as the training set and 20% as the test set. Due to the small number of defective target dataset, it is not divided into categories, but only into two categories of abnormal and normal, of which abnormal is mainly damage and dirt.

Training and testing configuration: the CPU model is AMD Ryzen 5 3600 6-Core Processor 3.59 GHz, the GPU model is NVIDIA Ge Force RTX 2060 8GB, the operating system is Windows 10, the CUDA version is 10.1, and the Pytorch version is 1.7.0.

The initial learning rate was set to 0.03, the total number of epochs was 500, and the batch size was 64. Other programs were closed during the test experiments to ensure that the effect of the environment on the measurement speed was reduced.

1) Target detection experiments. The results of the defective target detection experiments are shown in Table 3. In this section, several classical and excellent target detection networks are compared in the experiments, including one-stage YOLOv5, YOLOv7, and two-stage Faster R-CNN FPN, and the mAP obtained is generally very low, which indicates that it is difficult to detect efficiently with the limited data available.

Among them, the Faster R-CNN FPN has the highest mAP of 79.67%, indicating that the Faster R-CNN FPN can achieve high accuracy using RPN to extract vector features for classification. And the mAP of YOLOv7x is 52.49%, which is 20.12% less than YOLOv5x, indicating that YOLOv5 has higher generalization. The mAP of YOLOv5m, which is suitable for real-time detection, is 67.94%, which is 4.67% less than YOLOv5x.

The mAP of this paper's algorithm reaches up to 79.60%, which is only 0.07% different from the mAP value of Faster R-CNN FPN, but the AP bad (%) and AP normal (%) dimensions are higher than that of Faster R-CNN FPN, which is advantageous for defect extraction.

Table 3. Defect target test results

Various algorithms	mAP(%)	AP bad(%)	AP normal(%)
YOLOv5m	67.94	67.45	70.13
YOLOv5x	72.61	73.01	73.22
YOLOv7x	52.49	46.82	59.87
Faster R-CNN FPN	79.67	80.53	81.56
This algorithm	79.60	81.24	83.77

2) Classification experiment. The results of the defect classification experiments are shown in Table 4. Common classification networks were used in the experiments for testing, among which VGG, ResNet, ResNeXt, DenseNet, GoogLeNet belong to the deep networks, which are more computationally intensive.MnasNet, MobilNetv3, ShuffleNet and GhostNet belong to the lightweight networks, which are less computationally intensive. The table also shows the GFLOPs of different networks, the accuracy of different categories on the training and validation sets, the average time on the validation set.

In terms of GFLOPs, the deep networks are relatively large, with a maximum of 23.7 for VGG and a minimum of 0.11 for the algorithm in this paper.In terms of average time, the lightweight networks do not have the smallest test times, although their GFLOPs are generally small. The lightweight network MnasNet has the smallest test time of 6.7 ms. However, VGG, which has the largest GFOLPs, has a test time of only 6.8 ms, indicating that the optimization for ordinary convolution reduces the amount of computation though. However, the speed is not necessarily in platforms with medium computing power, and possesses good results in mobile platforms with small computing power.

In terms of overall accuracy, the accuracy of the training set, except on MnasNet, reaches more than 90%, and some even reach 100%, indicating that the network can basically fit the data in the training set.

In the validation set classification effect, the deep network is generally better than the lightweight network, in which the highest in the deep network is ResNeXt50, reaching 89.1%, and the algorithm proposed in this paper is 87.4. Based on the validation classification value of DenseNet, ResNet101, etc., it shows that the depth of the network reaches a certain degree, and the performance of this data is not very much related to the depth of the network model.

In summary, from the point of view of accuracy, the algorithm in this paper has the best detection performance, followed by ResNeXt50. While considering the balance of speed and accuracy, the algorithm in this paper, ResNet50 test the best performance.

Table 4. The results of the defect classification experiment

	Training			Validation			GFLOPs	Time(ms)
	Bad (%)	Normal (%)	All (%)	Bad (%)	Normal (%)	All (%)		
VGG	100.0	99.1	99.5	80.2	78.4	79.3	23.7	6.8
DenseNet201	100.0	100.0	100.0	87.3	81.2	84.1	5.2	27.3
Res Net50	99.1	99.3	99.4	79.5	83.3	80.5	4.6	6.5
Res Net101	99.1	100.0	100.0	84.2	86.4	86.3	8.9	12.4
Res Net152	99.2	100.0	99.2	77.3	91.2	84.2	12.4	16.9
Res NeXt50	99.3	100.0	100.0	87.4	90.0	89.1	4.5	9.6
Res NeXt101	100.0	100.0	100.0	81.2	86.4	84.7	17.3	22.5
GoogLeNet	90.5	99.3	91.5	67.3	85.3	77.2	1.3	7.8
MnasNet	77.3	82.4	79.3	65.6	64.2	65.3	0.35	6.7
MobilNetv3	88.6	96.5	92.1	52.4	64.5	69.5	0.21	8.9
ShuffleNetv2	95.3	98.7	98.6	45.3	62.8	55.2	0.66	7.2
GhostNet	93.5	96.3	95.2	66.1	70.4	69.4	0.15	12.3
This algorithm	98.6	98.4	95.3	69.5	78.7	87.4	0.11	10.4

3) Experiments based on target detection and classification. In the integrated defect recognition based on target detection and classification, two training approaches are proposed, and this section conducts experiments on the two training approaches. The comparison experiments of different training strategies are shown in Table 5.

In the table, the experiment evaluates the effect of different training approaches in two ways. One is the classification effect, the validation set used is the classification dataset, and the evaluation metric is the accuracy of different classes. The other is the target detection effect, the validation set used is the target detection dataset, and the evaluation metrics are precision, recall, and F1.

In the classification effect, the combined accuracy of the validation set of the embedded is 79.485% and the combined accuracy of the training set reaches 98.515%. The combined accuracy of the validation set for the morphing style is 75.46% and the combined accuracy of the training set reaches 86.94%. Thus the effect of embedded training approach is superior to that of the morphological training approach.

In the target detection effect, the maximum F1 is 66.15% for embedded and 49.57% for morphing style and embedded is 16.58% higher than morphing style. The difference between the two is larger than the classification accuracy gap. The results on the target detection dataset are poor because the classifiers trained using the shape-shifting style train only the object region, while the target detection dataset contains background interference.

Table 5. Comparison experiment of different training strategies

		Classification effect			Target detection effect		
		Normal (%)	Abnormality (%)	Synthesize (%)	Accuracy rate(%)	Recall rate(%)	F1(%)
Deformation type	Training	86.34	87.54	86.94	53.54	45.21	49.57
	validation	71.25	79.67	75.46			
Embedded	Training	97.03	100.0	98.515	69.87	66.87	66.15
	validation	79.22	79.75	79.485			

4. Conclusion

In this paper, for the problems encountered in the current distribution line quality acceptance project, the intelligent inspection technology of distribution line UAV and the automatic identification algorithm of inspection defects are proposed respectively. The experimental environment is set up to test the UAV distribution line training path planning algorithm based on key coordinate points. Using the processed distribution network defect image data, test the reinforcement learning-based distribution network inspection defect recognition algorithm.

1) A 30*30 experimental environment is set up for dynamic inspection path planning using the key coordinate point-based UAV distribution line path planning algorithm proposed in this paper. From the visualization results, it can be seen that in the 30 experiments conducted, the UAV nodes are able to complete the path planning tasks in different environments.

2) The image analysis acquired by the UAV is subjected to Gaussian denoising and histogram equalization algorithm for image enhancement. Establishing the distribution network defect data set, the algorithm proposed in this paper and Faster R-CNN FPN algorithm perform well in the target detection experiments, the mAP is 79.60% and 79.67%, respectively, and the algorithm has a good advantage in feature extraction. Meanwhile, in the defective target recognition inspection, the use of embedded training strategy can achieve better classification results.

Funding

Supported by Science and Technology Project of Guangxi Power Grid Co., Ltd.: Research on Key Technology of Panoramic Smart Insurance Power Supply System Based on Multi-Modal Artificial Intelligence Big Model and Decision Intelligence Technology (040100KC23110006).

References

[1] Kim, E., Lee, Y., He, L., Shin, K. G., & Lee, J. (2020). Power guarantee for electric systems using real-time scheduling. IEEE Transactions on Parallel and Distributed Systems, 31(8), 1783-1798.

[2] Wang, J., & Wei, R. (2023). Study on Urban Resilience Based on the Analysis of Supply Guarantee Facilities during Epidemic Closure—A Case Study of Shanghai in 2022. Open Journal of Civil Engineering, 13(1), 58-82.

[3] Mauree, D., Naboni, E., Coccolo, S., Perera, A. T. D., Nik, V. M., & Scartezzini, J. L. (2019). A review of assessment methods for the urban environment and its energy sustainability to guarantee climate adaptation of future cities. Renewable and Sustainable Energy Reviews, 112, 733-746.

[4] Aziz, S., Wang, H., & Peng, J. (2019). Guaranteed Load Power Supply based on Power Convection Coordination. Energy Procedia, 158, 6521-6526.

[5] Council, C. E. (2017). National energy guarantee. Council of Australian Governments (COAG) Energy Council, 7.

[6] Li, M., Hou, Y., Xie, Y., Jiang, S., Ye, D., & Zheng, G. (2022, December). A Selection Method of the Guaranteed Power Source for the Provincial Power Grid. In 2022 IEEE 5th Advanced Information Management, Communicates, Electronic and Automation Control Conference (IMCEC) (Vol. 5, pp. 342-347). IEEE.

[7] MURAD, C. A., Bellinello, M. M., Silva, A. J., Netto, A. C., de Souza, G. F. M., & Nabeta, S. I. Power Plants Maintenance Performance Indicators: A Novel Consolidated Corporate Approach Grounded on Rational Decision Method. GFM and Nabeta, SI, Power Plants Maintenance Performance Indicators: A Novel Consolidated Corporate Approach Grounded on Rational Decision Method.

[8] Sang, D., Yao, Y., Shi, D., & Cheng, C. (2024, May). Research on the characteristics of power supply and demand balance and supply guarantee strategies in new power system. In Eighth International Conference on Energy System, Electricity, and Power (ESEP 2023) (Vol. 13159, pp. 2182-2192). SPIE.

[9] Blaabjerg, F., Yang, Y., Yang, D., & Wang, X. (2017). Distributed power-generation systems and protection. Proceedings of the IEEE, 105(7), 1311-1331.

[10] Zhang, C., Qiu, Y., Chen, J., Li, Y., Liu, Z., Liu, Y., ... & Hwa, C. S. (2022). A comprehensive review of electrochemical hybrid power supply systems and intelligent energy managements for unmanned aerial vehicles in public services. Energy and AI, 9, 100175.

[11] Yun, H., Shim, H., & Ahn, H. S. (2019). Initialization-free privacy-guaranteed distributed algorithm for economic dispatch problem. Automatica, 102, 86-93.

[12] Wang, H., Huang, Z., Zhang, X., Huang, X., wei Zhang, X., & Liu, B. (2022). Intelligent power grid monitoring and management strategy using 3D model visual computation with deep learning. Energy Reports, 8, 3636-3648.

[13] Ding, T., Lin, Y., Bie, Z., & Chen, C. (2017). A resilient microgrid formation strategy for load restoration considering master-slave distributed generators and topology reconfiguration. Applied energy, 199, 205-216.

[14] Chen, S., Wen, H., Wu, J., Lei, W., Hou, W., Liu, W., ... & Jiang, Y. (2019). Internet of things based smart grids supported by intelligent edge computing. IEEE access, 7, 74089-74102.

[15] Tan, M., Yuan, S., Li, S., Su, Y., Li, H., & He, F. (2019). Ultra-short-term industrial power demand forecasting using LSTM based hybrid ensemble learning. IEEE transactions on power systems, 35(4), 2937-2948.

[16] Łukasik, Z., Kozyra, J., Kuśmińska-Fijałkowska, A., & Warchoł, R. (2018). Guaranteed power supply for the purpose of automated technological line of powder coating. Electrical Engineering, 100, 195-203.

[17] Peng, T., Yao, K., Xu, Y., Yang, C., Liu, Y., & Yang, X. (2023, October). A LADRC-based Control Strategy with Performance Guarantee for On-board SC ESS of Urban Rail Traction. In IECON 2023-49th Annual Conference of the IEEE Industrial Electronics Society (pp. 1-6). IEEE.

[18] Salman, A. D., Khalaf, O. I., & Abdulsahib, G. M. (2019). An adaptive intelligent alarm system for wireless sensor network. Indonesian Journal of Electrical Engineering and Computer Science, 15(1), 142-147.

[19] Farghali, M., Osman, A. I., Chen, Z., Abdelhaleem, A., Ihara, I., Mohamed, I. M., ... & Rooney, D. W. (2023). Social, environmental, and economic consequences of integrating renewable energies in the electricity sector: a review. Environmental Chemistry Letters, 21(3), 1381-1418.

[20] Carnero, M. C., & Gómez, A. (2017). Maintenance strategy selection in electric power distribution systems. Energy, 129, 255-272.

[21] Luchko, M. (2023). Hydrogen System of Autonomous Power Supply of Low Power. In Cooling Technologies-Technologies and Systems to Guarantee Thermal Comfort in Efficient Buildings. IntechOpen.

[22] Basciftci, B., Ahmed, S., & Gebraeel, N. (2020). Data-driven maintenance and operations scheduling in power systems under decision-dependent uncertainty. IISE transactions, 52(6), 589-602.

[23] Corcoran Evangeline,Denman Simon & Hamilton Grant. (2021). Evaluating new technology for biodiversity monitoring: Are drone surveys biased?. Ecology and Evolution(11),6649-6656.

[24] Ding Li & Chong Jiao. (2018). Research on the Key Technology of Survey Measurement Image Based on UAV. International Journal of Advanced Network, Monitoring and Controls(2),99-103.

[25] Bowen Ye,Sun Jin,Bing Li,Shuaiyu Yan & Deng Zhang. (2023). Dual Histogram Equalization Algorithm Based on Adaptive Image Correction. Applied Sciences(19).

[26] Li Yun,Zhang Yanmei,Ding Yanru,Jiang Shujuan & Yuan Guan. (2024). Correction to: A class integration test order generation approach based on Sarsa algorithm. Automated Software Engineering(1).

[27] Zhan Wei & Qu Shengqing. (2022). Cooperation Mode of Soccer Robot Game Based on Improved SARSA Algorithm. Wireless Communications and Mobile Computing.